Journal of Inorganic Biochemistry 104 (2010) 37–46

Contents lists available at ScienceDirect

Journal of Inorganic Biochemistry

journal homepage: www.elsevier.com/locate/jinorgbio

Dipeptide hydrolysis by the dinuclear zinc enzyme human renal dipeptidase: Mechanistic insights from DFT calculations

Rong-Zhen Liao [a,b], Fahmi Himo [b,*], Jian-Guo Yu [a,*], Ruo-Zhuang Liu [a]

[a] College of Chemistry, Beijing Normal University, Beijing 100875, People's Republic of China
[b] Department of Organic Chemistry, Arrhenius Laboratory, Stockholm University, SE-10691 Stockholm, Sweden

ARTICLE INFO

Article history:
Received 8 July 2009
Received in revised form 11 September 2009
Accepted 25 September 2009
Available online 1 October 2009

Keywords:
Dipeptidase
Dinuclear zinc enzymes
Reaction mechanism
Density functional theory

ABSTRACT

The reaction mechanism of the dinuclear zinc enzyme human renal dipeptidase is investigated using hybrid density functional theory. This enzyme catalyzes the hydrolysis of dipeptides and β-lactam antibiotics. Two different protonation states in which the important active site residue Asp288 is either neutral or ionized were considered. In both cases, the bridging hydroxide is shown to be capable of performing the nucleophilic attack on the substrate carbonyl carbon from its bridging position, resulting in the formation of a tetrahedral intermediate. This step is followed by protonation of the dipeptide nitrogen, coupled with C–N bond cleavage. The calculations establish that both cases have quite feasible energy barriers. When the Asp288 is neutral, the hydrolytic reaction occurs with a large exothermicity. However, the reaction becomes very close to thermoneutral with an ionized Asp288. The two zinc ions are shown to play different roles in the reaction. Zn1 binds the amino group of the substrate, and Zn2 interacts with the carboxylate group of the substrate, helping in orienting it for the nucleophilic attack. In addition, Zn2 stabilizes the oxyanion of the tetrahedral intermediate, thereby facilitating the nucleophilic attack.

1. Introduction

Human renal dipeptidase (hrDP) is a glycosyl phosphatidylinositol-anchored cell surface enzyme that catalyzes the hydrolysis of dipeptides with D-, L-, or dehydro-amino acids at the C-terminus (Scheme 1) [1–3]. It plays an important role in the *in vivo* renal metabolism of glutathione and leukotriene D4, and exhibits hydrolytic activities toward β-lactam antibiotics, such as penem and carbapenem [4–6]. The latter feature has led to the development of cilastatin as a reversible and specific inhibitor, which can be used as a probe for colon cancer [7,8].

hrDP is a homodimer, consisting of 369 residues in each subunit, linked by a disulfide [9,10]. It utilizes a dinuclear zinc site to catalyze the reaction [9,10]. It has a distorted $(\alpha/\beta)_8$-barrel structural fold, very similar to those of murine adenosine deaminase [11], bacterial *Klebsiella aerogenes* urease [12], and *Pseudomonas diminuta* phosphotriesterase [13]. The X-ray crystal structure of hrDP has been solved in both the unliganded form and in complex with the dipeptidyl moiety of the cilastatin inhibitor [10]. The two zinc ions in the active site (Fig. 1) are bridged by a glutamate residue (Glu215) and an oxygen species. In addition, three histidines (His20, His198, and His219) and an aspartate (Asp22) are coordinated to the dinuclear zinc center. Asp288, situated very close to Zn2, forms a hydrogen bond to the bridging oxygen. His152, a second-shell residue, is hydrogen-bonded to the peptide carbonyl oxygen, and is believed to contribute to the substrate recognition [10] Furthermore, the carboxylate terminus of the inhibitor is coordinated to Zn2 and hydrogen-bonded to Arg230 and Tyr255.

On the basis of the X-ray structure and earlier mutational studies, a plausible mechanistic proposal has been put forward [10]. The first step is the binding of the dipeptide substrate, in which the N-terminal amino group coordinates to Zn1, and the carboxylate group coordinates to Zn2, in a similar fashion as the cilastatin inhibitor in the crystal structure. Such a binding mode has been supported by molecular docking studies [14,15]. The bridging ligand is proposed to be a water molecule that then is deprotonated by Asp288, forming a bridging hydroxide [10]. This hydroxide in turn performs a nucleophilic attack on the dipeptide carbonyl carbon, leading to a tetrahedral intermediate. His152 is suggested to stabilize the oxyanion in the tetrahedral intermediate [10]. Subsequently, the peptide C–N bond is cleaved. Exactly how this is done is not known. It is possible that Asp288 shuttles a proton from the bridging oxygen to the peptide nitrogen, since similar reaction steps have been suggested for several related dinuclear zinc enzymes, such as β-lactamase from *Stenotrophomonas maltophilia* [16], methonine aminopeptidase from *Escherichia coli* [17], aminopeptidase from *Aeromonas proteolytica* [18], and dihydroorotase from *Escherichia coli* [19].

* Corresponding authors.
E-mail addresses: himo@organ.su.se (F. Himo), jianguo_yu@bnu.edu.cn (J.-G. Yu).

0162-0134/$ - see front matter © 2009 Published by Elsevier Inc.
doi:10.1016/j.jinorgbio.2009.09.025

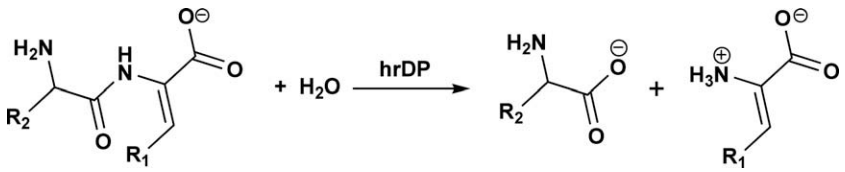

Scheme 1. Reaction catalyzed by hrDP.

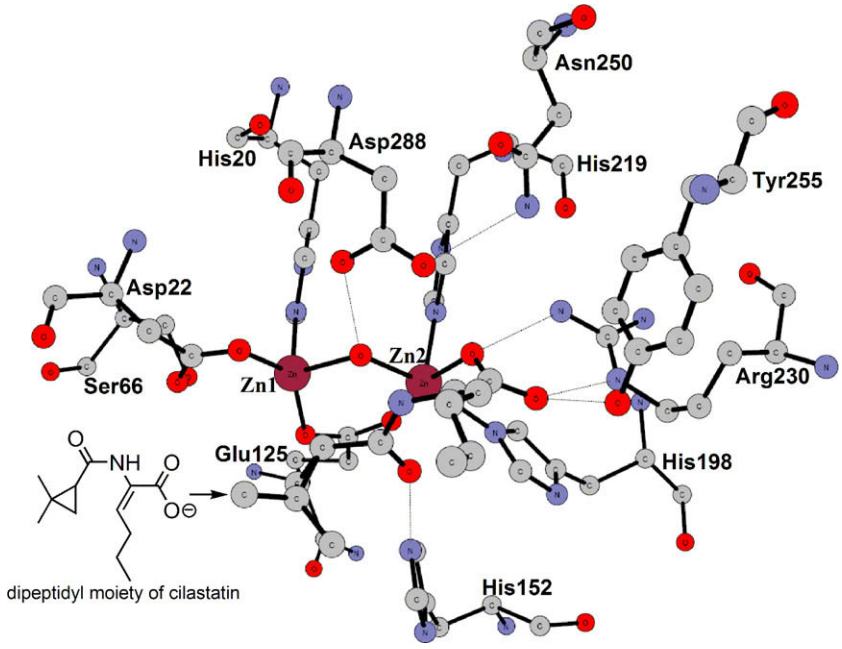

Fig. 1. X-ray structure of the active site of hrDP complexed with a dipeptidyl moiety of cilastatin. (coordinates taken from PDB entry 1ITU) [10].

In the above mechanistic proposal, the ionized Asp288 is assumed to accept the proton during the formation of the bridging hydroxide. However, it is quite conceivable that this proton is released to solution, and that Asp288 therefore would remain ionized. The protonation state of Asp288 might be crucial for the kinetics and thermodynamics of the catalytic reaction.

In the present study, we use quantum chemical methods to model the active site and to investigate the reaction mechanism of hrDP. With a model designed on the basis of crystal structure (PDB entry 1ITU) [10], the hybrid functional B3LYP [20,21], was employed to calculate the potential energy profile for this reaction with the Asp288 residue in either neutral or ionized state. We also consider the reaction of the cilastatin inhibitor and provide a rationalization for its low reactivity. This methodology has been successfully applied to study a wide array of enzymes, [22–27] including several related di-zinc enzymes [28–33].

2. Computational details

All calculations were performed using the hybrid density functional theory method B3LYP, as implemented in the Gaussian03 code [34]. Geometries were optimized with the 6-31G(*d, p*) basis set for the C, N, O, H elements and the effective core potential LANL2DZ [35] basis set for Zn. Based on these optimized geometries, more accurate energies were calculated with the larger basis set 6-311+G(*2d, 2p*) for all elements. The solvation effects from the protein surrounding that was not explicitly included in the quantum chemical cluster model were considered by performing single-point calculations on the optimized geometries at the same theory level as the optimization using the conductor-like polarizable continuum model (CPCM) method [36–39] with the default UA0 radii (united atom topological model). In this approach the surrounding protein is treated as a homogenous macroscopic continuum with some dielectric constant. Here, we used the standard value $\varepsilon = 4$.

Frequency calculations were performed at the same level of theory on all stationary points along the reaction path to calculate the zero-point energy (ZPE) effects. Some atoms are fixed to their X-ray positions (see below), which gives rise to several small imaginary frequencies, all below 50*i* cm^{-1}. These do not contribute significantly to the ZPE and thus can be ignored. However, they make the calculations of harmonic entropy effects inaccurate. Therefore, entropy was not considered in the present study.

3. Model of active site

To investigate the reaction mechanism, a quantum chemical model of the hrDP active site was designed on the basis of the X-ray structure solved for the enzyme in complex with cilastatin (PDB code 1ITU) [10]. The first coordination shell of the di-zinc site was represented by three methyl-imidazoles that mimic the His20, His198, and His219 residues and two acetates that represent the Asp22 and Glu125 residues. A hydroxide was used as the bridging nucleophile oxygen species. The important Asp288 was modeled in either the neutral (called **Case I**) or the ionized (called **Case II**) forms, using either acetate or acetic acid, respectively. Five important second-shell residues (Ser66, His152, Arg230, Asn250, and Tyr255) were also included, and modeled by methanol, methyl-

imidazole, N-methyl-guanidine, acetamide, and phenol, respectively. The inhibitor of the crystal structure was manually replaced with a dehydro Ala-Ala dipeptide substrate (see Fig. 2), which is adequate for the purpose of this mechanistic study. Hydrogen atoms were added manually. To keep the optimized structures close to the experimental one, the truncation atoms were kept

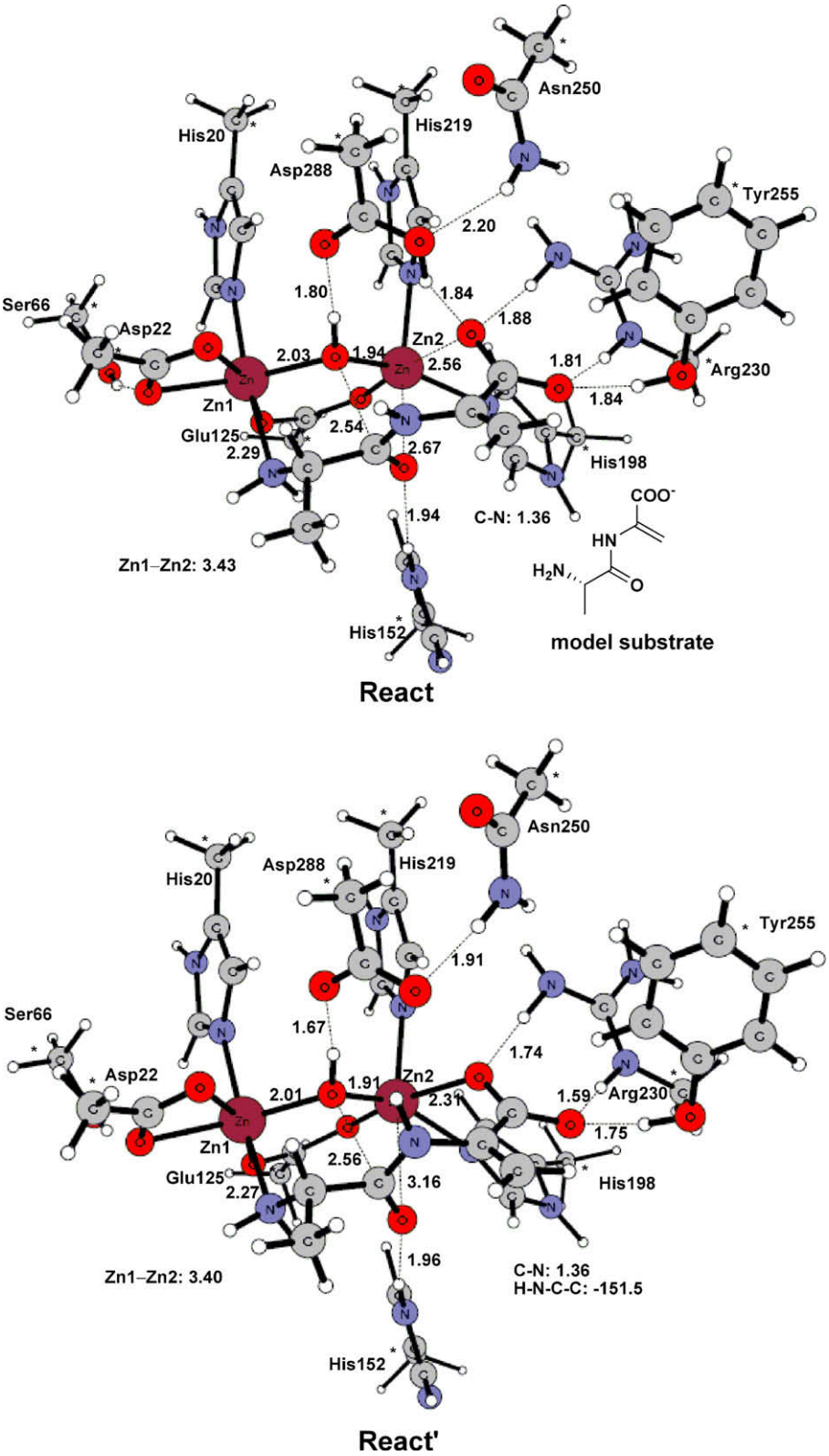

Fig. 2. Optimized structures for the active site model of hrDP in both neutral (**React**) and ionized (**React'**) forms of Asp288. Atoms marked with asterisks were fixed at their X-ray structure positions during the geometry optimizations. Distances are given in angstrom (Å).

fixed at their X-ray positions during the geometry optimizations. The fixed atoms are marked with asterisks in the figures below. The total size of the model with a neutral Asp288 is thus 136 atoms with a total charge of +1, while with the ionized Asp288 it is 135 atoms with a total charge of 0.

4. Results and discussion

In this study, we consider two scenarios in which Asp288 is either in the neutral or ionized form. The optimized structures of the active site models in complex with the model substrate for these two cases (here referred as **React** and **React′**, respectively) are displayed in Fig. 2. We first note that the N-terminal amino group is coordinated to Zn1, while the C-terminal carboxylate group is coordinated to Zn2 through one of its oxygens. This Zn1–amino interaction seems to be of importance for the hydrolysis, since the cilastatin inhibitor lacks both an amino group (as in dipeptide) and a hydroxyl group (as in β-lactam antibiotics) that might coordinate to Zn1. This is possibly a common feature for dinuclear zinc aminopeptidases, as it has also been suggested in three related enzymes, namely aminopeptidase from *Aeromonas proteolytica* (AAP) [29,40], methonine aminopeptidase from *Escherichia coli* (MetAP) [41], and bovine lens leucine aminopeptidase (bILAP) [42].

The substrate carboxylate group interacts with the side chains of the Arg230 and Tyr255 residues through three hydrogen bonds. Furthermore, His152 forms a hydrogen bond to the dipeptide carbonyl oxygen. These interactions help orienting the substrate, so that it is ready for subsequent nucleophilic attack. The Zn–Zn distance is calculated to be 3.43 Å and 3.40 Å in **React** and **React′**, respectively, which is in good agreement with the distance found in the crystal structure (3.29 Å).

4.1. Hydrolysis with a neutral Asp288

From **React**, the structures of the nucleophilic attack transition state (**TS1**) and the resulting tetrahedral intermediate (**Inter**) have been optimized (shown in Fig. 3). The barrier is calculated to be 11.6 kcal/mol, which upon inclusion of solvation ($\varepsilon = 4$) decreases somewhat to 9.7 kcal/mol. We notice that the nucleophilic attack occurs directly from the bridging position, similarly to other dinuclear zinc enzymes that we have studied previously, such as phosphotriesterase (PTE) [28], AAP [29], dihydroorotase (DHO) [30], glyoxalase II (GlxII) [31], acyl-homoserine lactone hydrolase (AHL lactonase) [32], and RNase Z [33]. At **TS1**, the nascent O_μ–C bond is 1.81 Å, which is decreased from 2.54 Å in **React**, and the peptide C–N and C–O bonds are elongated from 1.36 and 1.24 Å, to 1.41 and 1.29 Å, respectively. At **Inter**, these two bonds are further elongated to 1.47 Å and 1.33 Å, respectively, while the O_μ–C is shortened to 1.53 Å. Due to the development of negative charge at the peptide carbonyl oxygen, the interaction between Zn2 and this oxygen becomes stronger, as seen from the bond distance, which is shortened considerably from 2.67 Å in **React** to 2.20 Å in **TS1** and 2.08 Å in **Inter**. This implies that Zn2 ion provides catalytic power by stabilizing the transition state and the tetrahedral intermediate, thereby lowering the barrier for the nucleophilic attack. In addition, His152 forms a slightly stronger hydrogen bond to the carbonyl oxygen, as indicated by the decrease of hydrogen bond distance (1.94 Å in **React** and 1.88 Å in **Inter**, see Figs. 2 and 3). This supports previous suggestions based on crystal structure analysis, that the His152 residue provides further stabilization to the transition state and the tetrahedral intermediate. Compared to **React**, **Inter** has a calculated energy of 11.3 kcal/mol, which decreases to 9.1 kcal/mol when solvation is added. **Inter** is thus only 0.6 kcal/mol below **TS1**.

The following steps involve the protonation of the peptide nitrogen by Asp288 and the cleavage of the C–N bond. The calculations show that these two events take place in one concerted transition state (**TS2**), which is shown in Fig. 3. Similar proposals have been put forward for other zinc enzymes, thermolysin [43–45], carboxypeptidase A [46,47], glutamate carboxypeptidase [48], AAP [29], DHO [30], MetAP [41]. In these enzymes, an aspartate or a glutamate helps the protonation of the amide nitrogen. At **TS2**, the key distances of the proton to the peptide nitrogen and the Asp288 oxygen are 1.20 Å and 1.36 Å, respectively. The scissile C–N bond is 1.62 Å, slightly increased from 1.47 Å in **Inter**. It turns out that concomitant with this proton transfer and the C–N bond cleavage, the proton of the bridging oxygen transfers to Asp288, with the distances of the proton to O_μ and the Asp288 oxygen being 1.07 and 1.42 Å, respectively. The calculated energy of **TS2** is +14.3 kcal/mol compared to **React**. However, it decreases by 5 kcal/mol, to +9.3 kcal/mol, when solvation effects are added. The resulting structure corresponds to the dinuclear zinc cluster in complex with two amino acid products (**Prod**, Fig. 3). It is calculated to be 11.2 kcal/mol (8.6 kcal/mol including solvation) lower than **React**.

The energies are summarized in Fig. 4. As seen from the figure, the calculated energy difference between **TS1** and **TS2** is too small to allow us to unambiguously determine which one of them corresponds to the rate-limiting step. The experimental rate constants are found to be in the range of 8–1600 s^{-1} for various dipeptide substrates [49]. These can be converted to barriers in the range of 13–16 kcal/mol using classical transition state theory. Our calculated barriers are thus somewhat underestimated. Several sources of error can be envisioned here, such as the underlying DFT energies, the size of the model and the use of the coordination locking scheme, the homogeneous solvation model, and also the inherent inaccuracy in the X-ray crystal structure.

4.2. Hydrolysis with an ionized Asp288

The above calculations assume that the Asp288 residue is in the neutral form and can be used as a general acid to protonate the peptide bond, leading to its cleavage. However, it can be envisioned that this residue might instead be in the ionized (deprotonated) form. We therefore explored the hydrolysis mechanism also for this scenario (called **Case II**).

In **React′**, the Asp288 residue, now being negatively-charged, forms stronger hydrogen bonds to the bridging hydroxide and the neighboring Asn250 compared to **React**. In addition, there is a weak hydrogen bond between the Asp288 oxygen and the peptide NH (2.32 Å). Due to the lack of hydrogen bond between Asp288 and the carboxylate group of the substrate, the carboxylate oxygen in **React′** binds more strongly to Zn2 as compared to **React**.

The optimized structures of the transition state for the nucleophilic attack (**TS1′**) and the resulting tetrahedral intermediate (**Inter1′**) are displayed in Fig. 5. The critical geometric parameters of **TS1′** are quite similar to those of **TS1**. The nucleophilic attack occurs directly from a bridging position and the C–O_μ distance is 1.85 Å (1.81 Å in **TS1**). The energy barrier is calculated to be 10.8 kcal/mol, which after solvation is slightly increased to 11.0 kcal/mol. This barrier is comparable to that of **Case I** (9.7 kcal/mol after solvation). The resulting tetrahedral intermediate **Inter1′** lies at +9.7 kcal/mol relative to **React′** (7.1 kcal/mol with solvation). It is interesting to note that the hydrogen bond between the bridging hydroxide and Asp288 in **Inter1′** is considerably shorter than that in **Inter** (1.43 vs. 1.72 Å).

In **Case I**, we found that the proton transfer from the bridging hydroxide to Asp288, the proton transfer from Asp288 to the peptide nitrogen, and the C–N bond cleavage occur in the same transition state. For **Case II**, the calculations suggest that two more steps

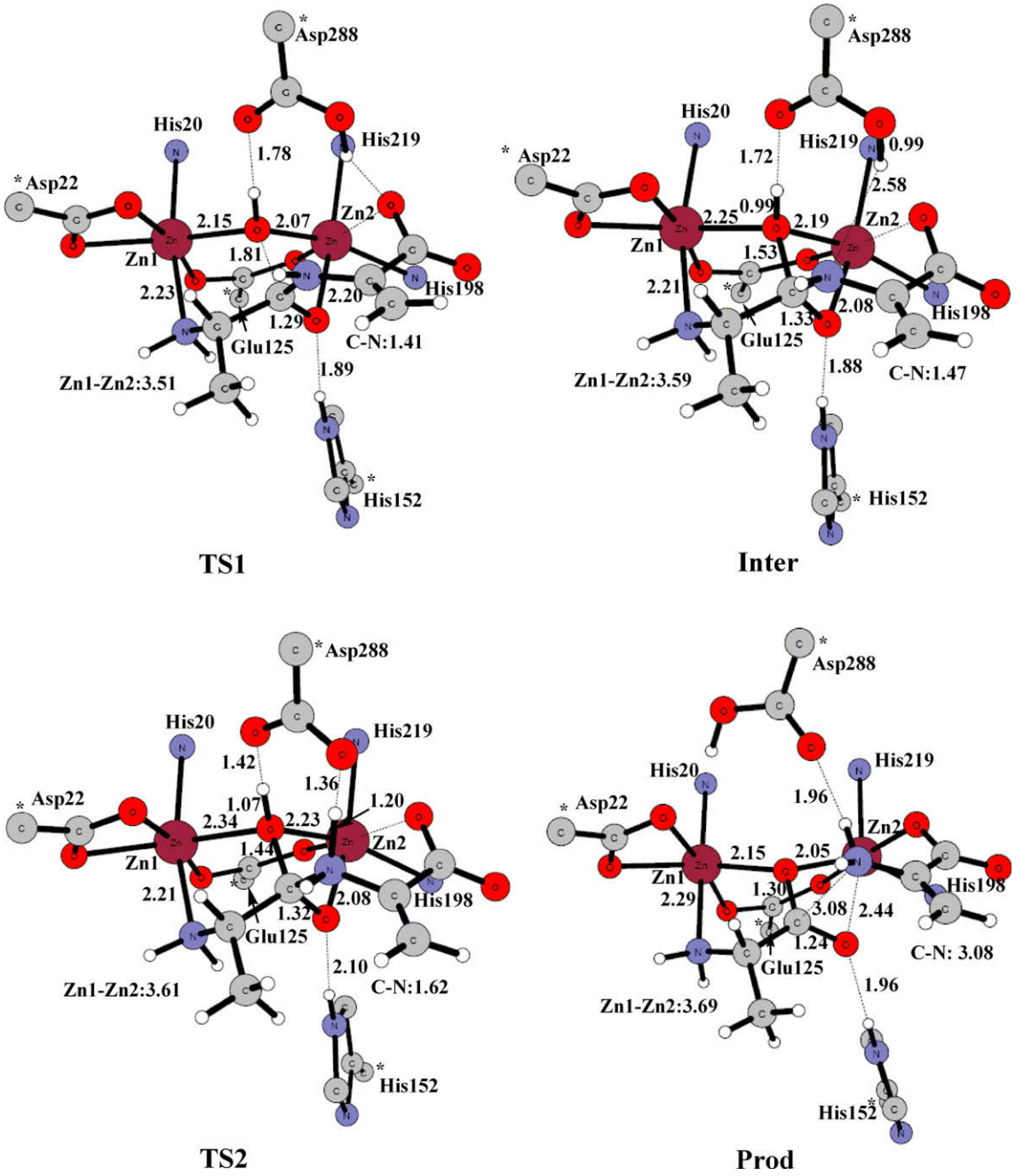

Fig. 3. Optimized geometries of stationary points along the reaction pathway in **Case I** with a neutral Asp288. For clarity, some residues and hydrogen atoms are not shown, and the imidazole ligands are represented by only a nitrogen atom in the figures.

are needed. First, the proton of the bridging hydroxide is transferred to Asp288. We have optimized the transition state, and the resulting intermediate (**TS2′** and **Inter2′**, respectively, see Fig. 5). This step is calculated to be very fast. In fact, **TS2′** is calculated to be 0.3 kcal/mol lower than **Inter1′**, which of course is an artifact of the technical procedures employed. It most likely originates from the fact that the geometries are optimized with a smaller basis set and the final energies are then calculated with a larger basis set. The potential energy profiles of two basis sets could be somewhat shifted relative each other, and when the barrier is extremely low, this could result in a slightly negative barrier. We have previously observed this for other dinuclear zinc enzyme [29].

The subsequent step is cleavage of hydrogen bond between the Asp288 oxygen and peptide NH and the inversion of the configuration of the peptide nitrogen, which prepares it to accept a proton from Asp288. The transition state (**TS3′**) and resulting intermediate (**Inter3′**) were also optimized and are depicted in Fig. 6. The dihedral angle of H–N–C_{α}–$C_{carbonyl}$ is −123.2° at **Inter2′**, and becomes 179.9° at **TS3′** and 152.9° at **Inter3′**. Like the previous step, this inversion is found to be very fast. The calculated barrier is 0.2 kcal/mol without solvation and −0.9 kcal/mol when solvation is included. Again, this is an error of the optimization and solvation procedures. The important result here is that these two steps are very fast.

The final step is the protonation of the peptide nitrogen, which turns out to be coupled with the C–N bond cleavage. The transition state was located, with a C–N distance of 1.76 Å (**TS4′**, Fig. 6). The barrier is calculated to be 2.4 kcal/mol relative to **Inter3′** (3.0 kcal/

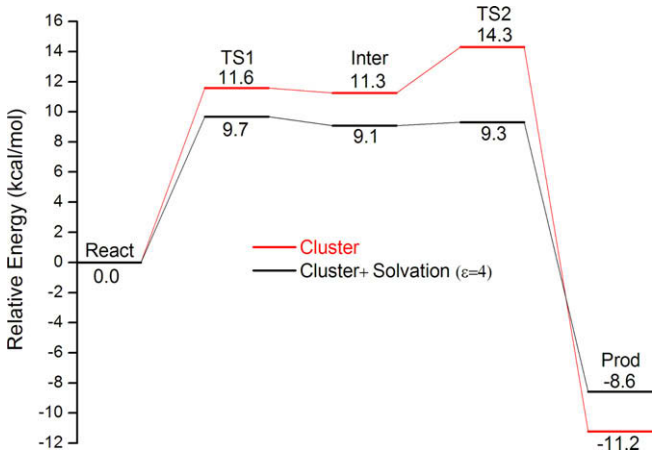

Fig. 4. Calculated potential energy profile for dehydro Ala-Ala dipeptide hydrolysis by hrDP in **Case I** with a neutral Asp288.

mol without solvation). In contrast to **Case I**, which is largely exothermic (8.6 kcal/mol), **Case II** is slightly endothermic, as the resulting enzyme–product complex (**Prod**′) is 1.0 kcal/mol higher than **React**′. The energies are summarized in Fig. 7.

As seen from Figs. 4 and 7, both cases, with Asp288 being neutral or ionized, have quite feasible and comparable barriers. This is quite different from two other dinuclear zinc enzymes, namely DHO [30] and MetAP [41]. In DHO, besides the bridging hydroxide and the Asp250 residue (which corresponds to Asp288 in hrDP), the two zinc ions have only one additional negatively-charged first-shell ligand, a carboxylated Lys102. Calculations have shown that if the Asp250 is neutral, the nucleophilicity of the bridging hydroxide may not be sufficient enough to perform the nucleophilic attack, and the barrier therefore is quite high. Therefore, an ionized Asp250 is preferable in DHO [30]. In MeAP, besides the bridging hydroxide and the Glu204 residue, the two zinc ions have three additional negatively-charged first-shell ligands, Asp97, Asp108, and Glu235. When Glu204 is ionized, Zn2 can not provide

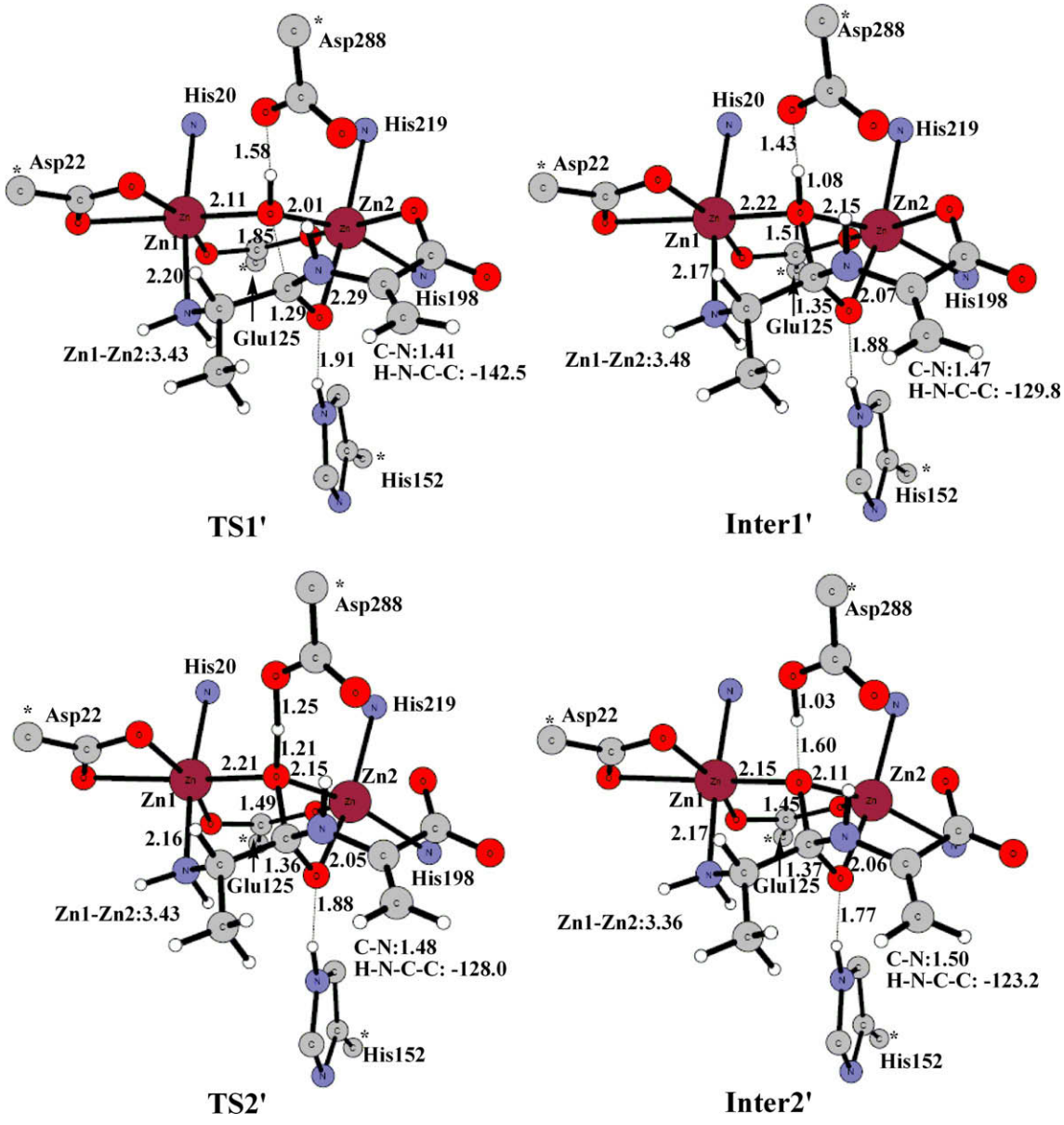

Fig. 5. Optimized geometries of the transition states and intermediates for the nucleophilic attack and the proton transfer from the bridging hydroxide to Asp288 in the case of an ionized Asp288.

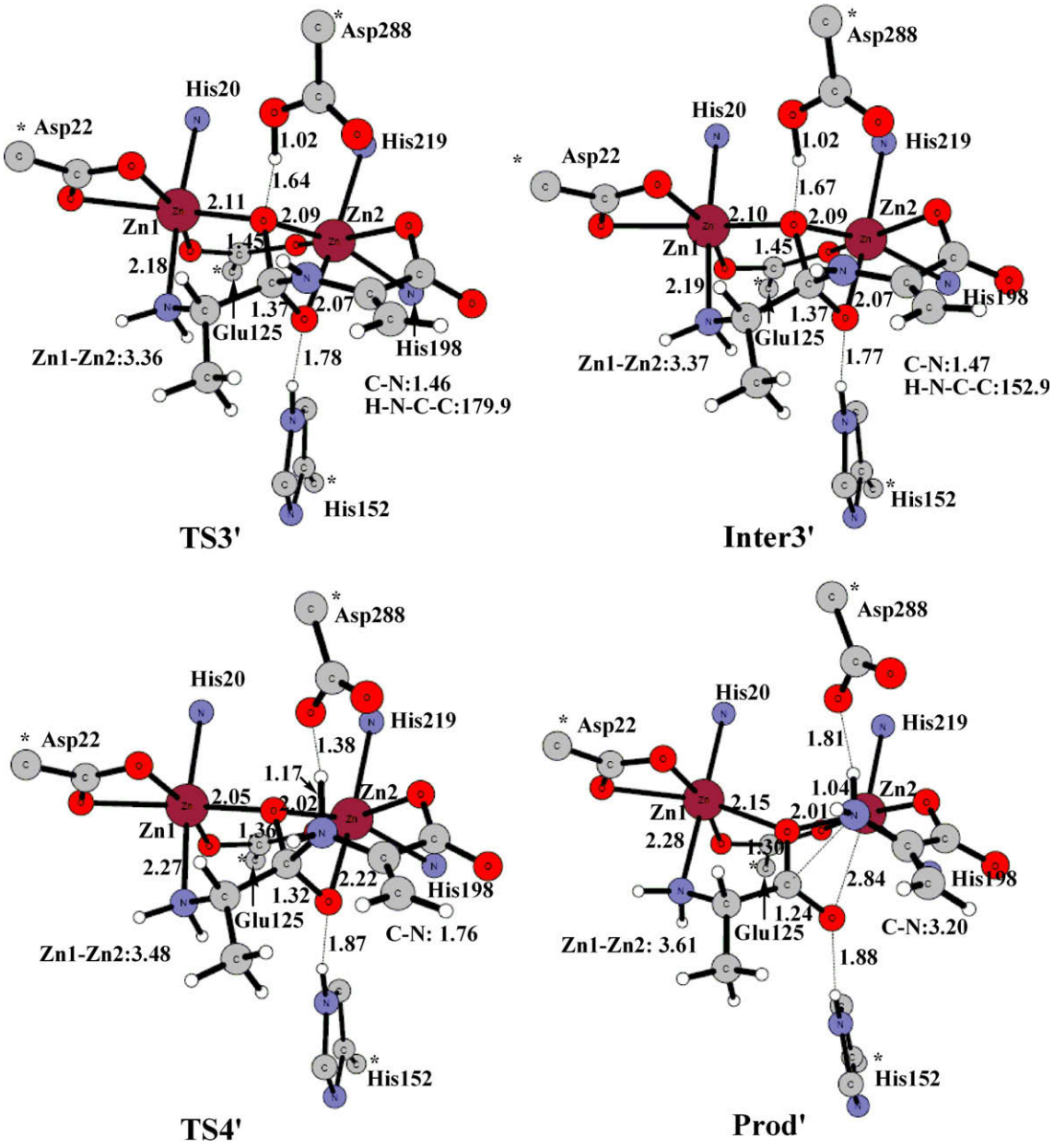

Fig. 6. Optimized geometries of the transition states, intermediates and product along the reaction pathway in the case of an ionized Asp288.

enough electrostatic stabilization on the oxygen anion during the nucleophilic attack. Hence, a neutral Glu204 is preferable for MeAP [41]. The situation for hrDP seems to be between DHO and MeAP, since there are two additional negatively-charged first-shell ligands (Asp22 and Glu125) bound to the dinuclear zinc center. The protonation state of the Asp288 is not crucial for the enzymatic activity, as shown from the calculations presented above.

4.3. Hydrolysis of cilastatin inhibitor

Based on the crystal structure, it was suggested that the interactions between the cyclopropyl group of cilastatin and Tyr68 and between the alkyl group of cilastatin and Tyr252 prevent departure of the leaving group from the tetrahedral intermediate. Therefore, cilastatin is an inhibitor and not a substrate for hrDP [14]. Here we use the same active site model as above, with a neutral Asp288, and a model of cilastation (see Fig. 8) to study the hydrolysis reaction of this compound. The quantitative computa-

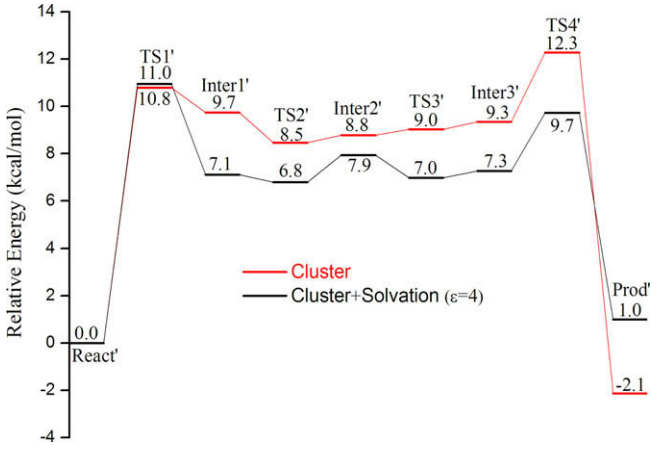

Fig. 7. Calculated potential energy profile for dehydro Ala-Ala dipeptide hydrolysis by hrDP in **Case II**.

tional treatment of these effects requires of course a much larger model of the active site. Many more groups need to be included in order to obtain a proper description of the steric effects of the active site.

The reaction mechanism is very similar to that for natural substrate hydrolysis as shown above. However, the barrier for the nucleophilic attack (15.6 kcal/mol with solvation and 24.2 kcal/mol without), and the barrier for the second step (15.9 and 26.6 kcal/mol with and without solvation correction, respectively) are significantly higher (Fig. 9). From the calculations, we can see a couple of reasons. First, the repulsion between Zn1 and the cyclopropyl group of cilastatin becomes stronger in going from **React**″

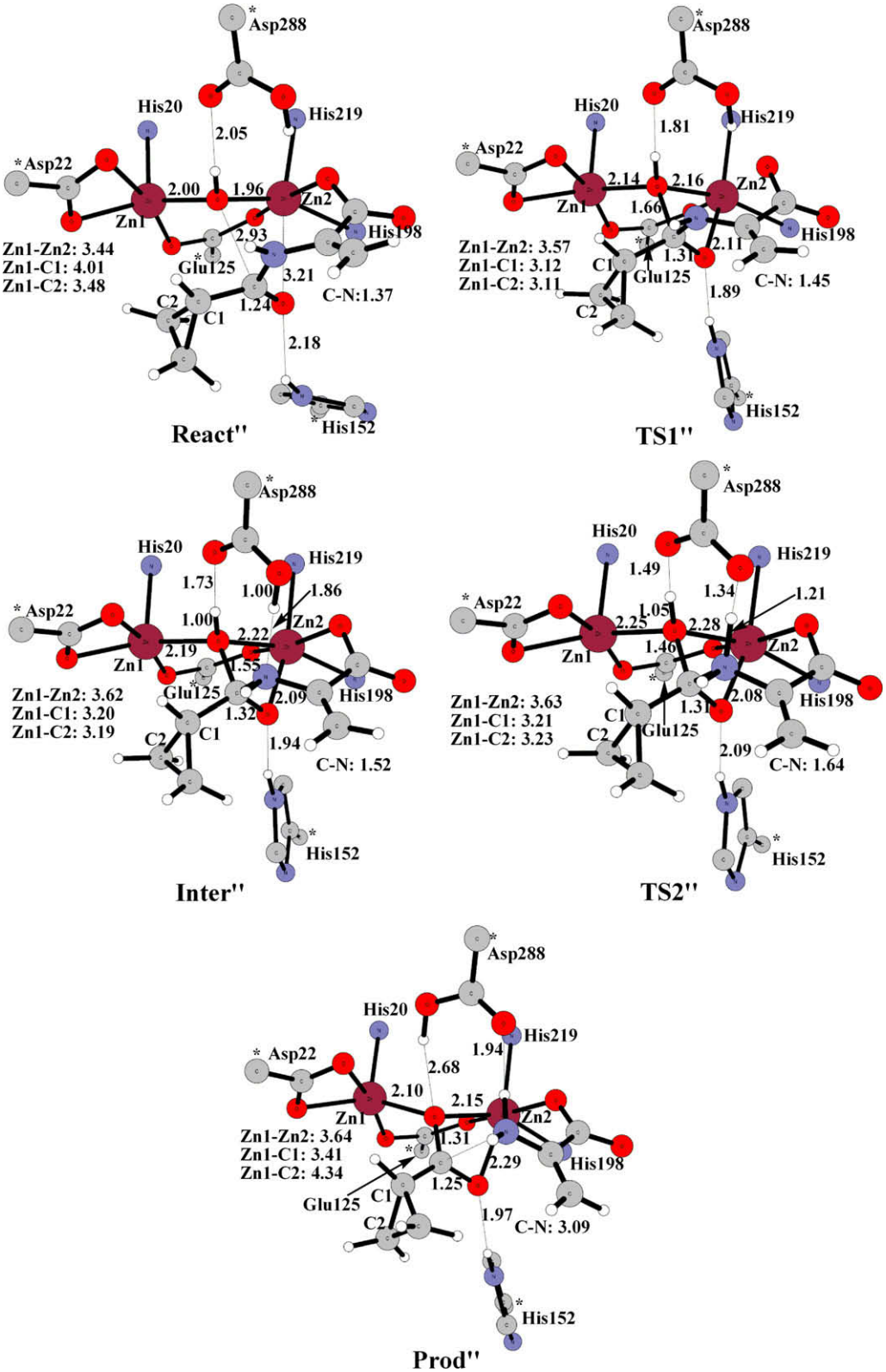

Fig. 8. Optimized geometries of stationary points along the reaction pathway for cilastatin hydrolysis.

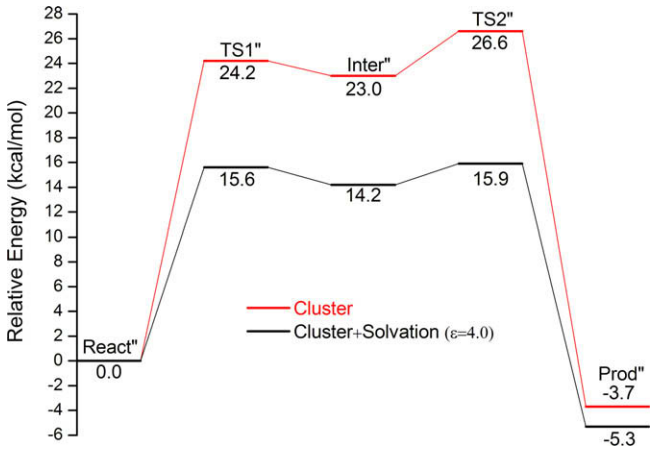

Fig. 9. Calculated potential energy profile for cilastatin hydrolysis by hrDP.

to **TS1**″ and **TS2**″, as seen from the Zn1–C1 and Zn1–C2 distances (see Fig. 8). Second, the repulsion between Zn1 and the cyclopropyl group of cilastatin make the carbonyl group of cilastatin slightly further away from the bridging hydroxide in the reactant (O–C is 2.93 Å in **React**″ compared to 2.54 Å in **React**). These results explain, in part, why cilastatin is an inhibitor and not a substrate. Considerably larger models are required to get a more complete picture, which is beyond the scope of this study.

5. Conclusions

In the present paper, we have investigated the reaction mechanism of the dinuclear zinc enzyme hrDP using a quantum chemical model of the active site. Two mechanistic scenarios based on the protonation state of Asp288 were considered. The optimized geometries of the stationary points are displayed in Figs. 2, 3, 5 and 6, and the calculated potential energy profiles are shown in Figs. 4 and 7. The calculations support the previously proposed mechanism and provide a more detailed picture of the chemical steps involved in the reaction. To summarize, the following mechanistic features can be established from the calculations.

Both zinc ions are involved in substrate binding, with the amino group binding to Zn1 and the carboxylate group binding to Zn2. The Zn–amino interaction might be a common feature for dinuclear zinc aminopeptidases. Hydrogen bonding to His152, Arg230, and Tyr255 also helps orienting the substrate.

The bridging hydroxide performs the nucleophilic attack on the peptide carbonyl carbon directly from its bridging position, without the need to become terminal first. This is similar to several other dinuclear zinc enzymes studied previously, such as, PTE [28], AAP [29], DHO [30], GlxII [31], AHL lactonase [32], and RNase Z [33].

Zn2, along with His152, stabilize the oxygen anion during the nucleophilic attack, thereby lowering the energy barrier. Asp288 helps the protonation of the peptide nitrogen, facilitating the C–N cleavage. One of the important conclusions of the present calculations is that both the nucleophilic attack and the C–N bond cleavage can take place with Asp288 being either neutral or ionized. The energy barriers for both cases are quite similar (Fig. 4 and 7).

Furthermore, the barriers for the nucleophilic attack and the C–N bond cleavage are too close to make a safe conclusion about which one is the rate-limiting step.

Finally, despite the relatively small size of the active site model, the calculations were able to reproduce the fact that the cilastatin inhibitor has significantly higher barrier than the substrate. A couple of reasons for this were discussed.

6. Abbreviations

hrDP	human renal dipeptidase
CPCM	conductor-like polarizable continuum model
ZPE	zero-point energy
AAP	aminopeptidase from *Aeromonas proteolytica*
MetAP	methonine aminopeptidase
blLAP	bovine lens leucine aminopeptidase
PTE	phosphotriesterase
DHO	dihydroorotase
GlxII	glyoxalase II
AHL lactonase	acyl-homoserine lactone hydrolase

Acknowledgments

F. H. gratefully acknowledges financial support from The Swedish National Research Council (VR), The Carl Trygger Foundation, and The Magn Bergvall Foundation. This work was also supported by grants from the National Natural Science Foundation of China (Grant Nos. 20733002 and 20873008) and Major State Basic Research Development Programs (Grant Nos. 2004CB719903 and 2002CB613406).

References

[1] H. Adachi, Y. Tawaragi, C. Inuzuka, I. Kubota, M. Tsujimoto, T. Nishihara, H. Nakazato, J. Biol. Chem. 265 (1990) 3992–3995.
[2] I.J. White, J. Lawson, C.H. Williams, N.M. Hooper, Anal. Biochem. 268 (1999) 245–251.
[3] D. Rajotte, E. Ruoslahti, J. Biol. Chem. 274 (1999) 11593–11598.
[4] H.S. Kim, B.J. Canpbell, Biochem. Biophys. Res. Commun. 108 (1982) 1638–1642.
[5] B.J. Campbell, L.J. Forrester, W. Zahler, M. Burks, J. Biol. Chem. 259 (1984) 14586–14590.
[6] H. Kropp, J.G. Sundelof, R. Hajdu, F.M. Kahan, Antimicrob. Agents Chemother. 22 (1982) 62–70.
[7] F.M. Kahan, H. Kropp, J.G. Sundelof, J. Birnbaum, J. Antimicrob. Chemother. 12 (1983) 1–35.
[8] P. Buckhaults, C. Rago, B.S. Croix, K.E. Romans, S. Saha, L. Zhang, B. Vogelstein, K.W. Kinzler, Cancer Res. 61 (2001) 6996–7001.
[9] Y. Nitanai, Y. Satow, H. Adachi, M. Tsujimoto, J. Cryst. Growth 168 (1996) 280–283.
[10] Y. Nitanai, Y. Satow, H. Adachi, M. Tsujimoto, J. Mol. Biol. 321 (2002) 177–184.
[11] Z. Wang, F.A. Quiocho, Biochemistry 37 (1998) 8314–8324.
[12] E. Jabri, M.B. Carr, R.P. Hausinger, P.A. Karplus, Science 268 (1995) 998–1004.
[13] M.M. Benning, S.B. Hong, F.M. Raushel, E.M. Holden, J. Biol. Chem. 275 (2000) 30556–30560.
[14] T.P. Smyth, J.G. Wall, Y. Nitanai, Bioorg. Med. Chem. 11 (2003) 991–998.
[15] M. Kim, J. Kim, E. Jung, K. Choi, J.-M. Shin, S.-K. Kang, M.-K. Kim, Y.-J. Choi, S.-H. Choi, Mol. Simulat. 33 (2007) 495–503.
[16] J. Spencer, J. Read, R.B. Sessions, S. Howell, G.M. Blackburn, S.J. Gamblin, J. Am. Chem. Soc. 127 (2005) 14439–14444.
[17] W.T. Lowther, Y. Zhang, P.B. Sampson, J.F. Honek, B.W. Mattews, Biochemistry 38 (1999) 14810–14819.
[18] W. Desmarais, D.L. Bienvenue, K.P. Bzymek, G.A. Petsko, D. Ringe, R.C. Holz, J. Biol. Inorg. Chem. 11 (2006) 398–408.
[19] J.B. Thoden, G.N. Phillips Jr., T.M. Neal, F.M. Raushel, H.M. Holden, Biochemistry 40 (2001) 6989–6997.
[20] A.D. Becke, J. Chem. Phys. 98 (1993) 5648–5652.
[21] C. Lee, W. Yang, R.G. Parr, Phys. Rev. B 37 (1988) 785–789.
[22] F. Himo, P.E.M. Siegbahn, Chem. Rev. 103 (2003) 2421–2456.
[23] L. Noodleman, T. Lovell, W.-G. Han, J. Li, F. Himo, Chem. Rev. 104 (2004) 459–508.
[24] P.E.M. Siegbahn, T. Borowski, Accounts. Chem. Res. 39 (2006) 729–738.
[25] F. Himo, Theor. Chem. Accounts 116 (2006) 232–240.
[26] M.J. Ramos, P.A. Fernandes, Accounts Chem. Res. 41 (2008) 689–698.
[27] P.E.M. Siegbahn, F. Himo, J. Biol. Inorg. Chem. 14 (2009) 643–651.
[28] S.-L. Chen, W.-H. Fang, F. Himo, J. Phys. Chem. B 111 (2007) 1253–1255.
[29] S.-L. Chen, T. Marino, W.-H. Fang, N. Russo, F. Himo, J. Phys. Chem. B 112 (2008) 2494–2500.
[30] R.-Z. Liao, J.-G. Yu, F.M. Raushel, F. Himo, Chem. Eur. J. 14 (2008) 4287–4292.
[31] S.-L. Chen, W.-H. Fang, F. Himo, J. Inorg. Biochem. 103 (2009) 274–281.
[32] R.-Z. Liao, J.-G. Yu, F. Himo, Inorg. Chem. 48 (2009) 1442–1448.
[33] R.-Z. Liao, F. Himo, J.-G. Yu, R.-Z. Liu, Eur. J. Inorg. Chem. 20 (2009) 2967–2972.

[34] Gaussian03, Revision D.01, M.J. Frisch, G.W. Trucks, H.B. Schlegel, G.E. Scuseria, M.A. Robb, J.R. Cheeseman, J.A. Montgomery, Jr., T. Vreven, K.N. Kudin, J.C. Burant, J.M. Millam, S.S. Iyengar, J. Tomasi, V. Barone, B. Mennucci, M. Cossi, G. Scalmani, N. Rega, G.A. Petersson, H. Nakatsuji, M. Hada, M. Ehara, K. Toyota, R. Fukuda, J. Hasegawa, M. Ishida, T. Nakajima, Y. Honda, O. Kitao, H. Nakai, M. Klene, X. Li, J.E. Knox, H. P. Hratchian, J. B. Cross, C. Adamo, J. Jaramillo, R. Gomperts, R. E. Stratmann, O. Yazyev, A.J. Austin, R. Cammi, C. Pomelli, J.W. Ochterski, P.Y. Ayala, K. Morokuma, G.A. Voth, P. Salvador, J.J. Dannenberg, V.G. Zakrzewski, S. Dapprich, A.D. Daniels, M.C. Strain, O. Farkas, D.K. Malick, A.D. Rabuck, K. Raghavachari, J.B. Foresman, J.V. Ortiz, Q. Cui, A.G. Baboul, S. Clifford, J. Cioslowski, B.B. Stefanov, G. Liu, A. Liashenko, P. Piskorz, I. Komaromi, R.L. Martin, D.J. Fox, T. Keith, M.A. Al-Laham, C.Y. Peng, A. Nanayakkara, M. Challacombe, P.M.W. Gill, B. Johnson, W. Chen, M.W. Wong, C. Gonzalez, J.A. Pople, Gaussian, Inc., Pittsburgh, PA, 2004.
[35] P.J. Hay, W.R. Wadt, J. Chem. Phys. 82 (1985) 270–283.
[36] A. Klamt, G. Schüürmann, J. Chem. Soc., Perkin. Trans. 2 (1993) 799–805.
[37] J. Andzelm, C. Kölmel, A. Klamt, J. Chem. Phys. 103 (1995) 9312–9320.
[38] V. Barone, M. Cossi, J. Phys. Chem. A 102 (1998) 1995–2001.
[39] M. Cossi, N. Rega, G. Scalmani, V. Barone, J. Comput. Chem. 24 (2003) 669–691.
[40] G. Schürer, H. Lanig, T. Clark, Biochemistry 43 (2004) 5414–5427.
[41] M. Leopoldini, N. Russo, M. Toscano, J. Am. Chem. Soc. 129 (2007) 7776–7784.
[42] G. Schürer, A.H.C. Horn, P. Gedeck, T. Clark, J. Phys, Chem. B 106 (2002) 8815–8830.
[43] S. Antonczak, G. Monard, M. Ruiz-López, J.-L. Rivail, J. Mol. Model. 6 (2000) 527–538.
[44] V. Pelmenschikov, M.R.A. Blomberg, P.E.M. Siegbahn, J. Biol. Inorg. Chem. 7 (2002) 284–298.
[45] J. Blumberger, G. Lamoureux, M.L. Klein, J. Chem, Theory Comput. 3 (2007) 1837–1850.
[46] M.W.Y. Szeto, J.I. Mujika, J. Zurek, A.J. Mulholland, J.N. Harvey, J. Mol. Struct. (THEOCHEM) 898 (2009) 106–114.
[47] D. Xu, H. Guo, J. Am. Chem. Soc. 131 (2009) 9780–9788.
[48] V. Klusák, C. Bařinka, A. Plenchanovová, P. Mlčochová, J. Konvalinka, L. Rulíšek, J. Lubkowski, Biochemistry 48 (2009) 4126–4138.
[49] T. Watanabe, Y. Kera, T. Matsumoto, R. Yamada, Biochim. Biophys. Acta 1298 (1996) 109–118.